Photodissociation of Bidentate Metal Complex Cations−Hydrogen Shift Reactions

Haichuan Liu, Julong Sun, and Shihe Yang*

Department of Chemistry, The Hong Kong University of Science and Technology, Clear Water Bay, Kowloon, Hong Kong, China

Received: March 25, 2003; In Final Form: May 9, 2003

Photoinduced reactions of bidentate metal complexes Mg^+(2-methoxyethanol), Mg^+(1,2-dimethoxyethane), and Mg^+(1,2-diaminoethane) have been studied combining mass-selective photodissociation spectroscopy and quantum mechanical calculations. Besides the evaporative fragment cation Mg^+, copious reactive channel photoproduct cations have been identified, which are propagated from the well-defined bidentate chelation structures upon photoexcitation of Mg^+. For Mg^+(2-methoxyethanol) and Mg^+(1,2-dimethoxyethane), most reactive channel photoproducts are actually Mg^+−molecule complexes, such as $Mg^+(H_2O)$, $Mg^+(HCHO)$, $Mg^+(CH_3OH)$, $Mg^+(C_2H_6O)$, etc. with an exception of Mg^+OH. The reactive channel photoproducts of Mg^+(1,2-diaminoethane) consist of a cationic complex $Mg^+(H_2NCH_3)$ and two other cations $CH_2NH_2^+$ and Mg^+NH_2, which are formed from the cleavage of the C−C and C−N bonds, respectively. Action spectra and branching fractions of all of the observed photofragments have been measured in a broad spectral range of 230−440 nm and analyzed against ab initio calculations. A hydrogen shift mechanism is proposed, whereby a critical hydrogen-shift step opens doors to the subsequent reactions. This mechanism appears to run through most photoreactions of the three complexes.

Introduction

The study of complexes of metal ions and organic molecules[1−25] is crucial to the understanding of biological processes that involve metal−protein or metal−peptide interactions.[26−32] During the past few years, we have used the photodissociation technique to study a series of complexes consisting of Mg^+ and organic halide and amine molecules.[33,34] The primary motivation for the experiments was to probe the chemistry in these well-defined complexes induced by the optical excitation of the unpaired electron in the metal cation Mg^+. This powerful technique allows us not only to probe the complex structures but also to study the reactions in a controlled fashion. Very interesting photoreactions have been observed concerning the activation of C−F, N−H, C−H, and C−N bonds with product channel selectivity and/or excitation state specificity.[33,34]

Recently, we have started to look into bidentate complexes in view of the fact that bidentate or polydentate chelations are often encountered in protein systems and play important roles in enzymatic functions, among other things. Initially, complexes of some fluoride molecules have been studied.[33a] This has led to the facile production of benzyne radical cations and the recognition of the orbital alignment effect on photoreactions in some complexes. Although the results are certainly interesting, metal−F interactions have limited implications to biological processes. In this paper, we report photoinduced reactions in complexes between Mg^+ and $HOCH_2CH_2OCH_3$, $CH_3OCH_2CH_2OCH_3$, and $H_2NCH_2CH_2NH_2$, in which the OH(R) and $NH(R)_2$ functional groups are ubiquitous in biological systems.

Information on the ground-state structures and energetics of some bidentate complexes has been obtained. Armentrout et al. have measured the accurate bond dissociation energies (BDEs) of M^+(1,2-dimethoxyethane)$_n$, $n = 1$ and 2, M^+(12-crown-4) where M = Li, Na, K, Rb, and Cs in a guided ion beam apparatus.[17b−e] Using ion cyclotron resonance (ICR) mass spectrometry and tandem quadruple mass spectrometry, Dearden and co-workers have investigated the interactions between alkali ions and crown ethers and acyclic glymes.[35]

The past decade has witnessed extensive efforts on elucidating the dissociation mechanisms of ionized ethylene glycol (or 1,2-ethanediol, $HOCH_2CH_2OH^{\bullet+}$),[36−38] 2-methoxyethanol ($HOCH_2CH_2OCH_3^{\bullet+}$),[38,39−41] 1,2-dimethoxyethane ($CH_3OCH_2CH_2OCH_3^{\bullet+}$),[42,43] diaminoethane ($H_2NCH_2CH_2NH_2^{\bullet+}$),[44] as well as other alkanediol and alkanediamine radical cations.[37,38,41,43,45] For the dissociation of alkanediol radical cations and their derivatives, at least four different mechanisms have been proposed.[36−46] Two of the mechanisms are deemed more reasonable or reliable, which are associated, respectively, with the "ion-dipole complex" and "distonic ion" intermediates.[36−39,40,42,43] In both mechanisms, double hydrogen transfer (DHT) is required,[37,38] e.g., to generate the $CH_3OH_2^+$ cation from the ethylene glycol radical cation. The "ion-dipole complex" mechanism is believed to be at work in the dissociation of $HOCH_2CH_2OH^{\bullet+}$ and $HOCH_2CH_2OCH_3^{\bullet+}$, in which the first step involves the C−C bond cleavage.[36−41] Even for this mechanism, different resultant intermediates have been proposed. One is the hydrogen-bridged intermediate,[40,41] and the other is the C−O−C−O moiety from the isomerization of the O−C−C−O backbone.[38] On the other hand, in the "distonic ion" mechanism,[38,42,43] hydrogen shift is the first step. For instance, in the fragmentation of $CH_3OCH_2CH_2OCH_3^{\bullet+}$, the 1,5-hydrogen shift results in an intermediate distonic ion $^{\bullet}CH_2OCH_2CH_2O^+(H)CH_3$.[42] However, no unified mechanism has been established so far to explain the dissociation behavior of the diol radical cation family. For example, although the fragmentation of $HOCH_2CH_2OC_2H_5^{\bullet+}$ and $C_2H_5OCH_2CH_2OC_2H_5^{\bullet+}$ also begins with the 1,5-H transfer, further dissociation behaviors are very different from that of $CH_3OCH_2CH_2OCH_3^{\bullet+}$.[43]

To complicate the issue further, a recent study using density functional theory (DFT) and threshold photoelectron−photoion coincidence spectroscopy (TPEPICO) verified neither of the two

* To whom correspondence should be addressed. E-mail: chsyang@ust.hk.

10.1021/jp034757z CCC: $25.00
Published on Web 07/09/2003

intermediates hypothesized in the "ion-dipole complex" mechanism mentioned above for the dissociation of $HOCH_2CH_2OH^{\bullet+}$.[36] Instead, the researchers concluded that the production of the $CH_3OH_2^+$ cation proceeds by tunneling through a potential barrier associated with an H-atom transfer. For the dissociation of the 1,2-diaminoethane radical cation ($H_2NCH_2CH_2NH_2^{\bullet+}$), the mechanism seems to be better understood. Bouchoux and co-workers proposed that, at a low internal energy, dissociation of $H_2NCH_2CH_2NH_2^{\bullet+}$ starts with 1,3-hydrogen transfer accompanied by the formation of an intermediate $H_2NCHCH_2NH_3^{\bullet+}$, prior to the loss of ammonia.[44] With higher internal energies, $H_2NCH_2CH_2NH_2^{\bullet+}$ tends to dissociate rapidly by the direct C−C bond rupture, forming the $CH_2{=}NH_2^+$ ion.

A distinctive feature of our work is that we start reactions from well-defined reactant configurations by forming complexes of $Mg^+(HOCH_2CH_2OCH_3)$, $Mg^+(CH_3OCH_2CH_2OCH_3)$, and $Mg^+(H_2NCH_2CH_2NH_2)$. The Mg^+ cation plays multiple roles as a structure-defining moiety, an energy-harvesting antenna, an active participant, and a reaction product reporter. It is hoped that such a strategy would allow us to probe the photoreactions of these relatively large systems in a controlled fashion. A number of photoproducts of these bidentate complexes have been identified in the photodissociation experiments. With the help of quantum mechanics calculations, we have proposed a general mechanism that embodies a crucial hydrogen transfer step, which breaks paths for the subsequent reactions.

Experimental Section

The cluster apparatus for the present experiments has been described elsewhere,[33] so only a brief description is given here. A rotating magnesium rod (5 mm in diameter and 5 cm in length) attached to a motor was mounted 15 mm downstream from the exit of a pulsed valve (General Valve). Driven by the step motor, the sample rod rotated by screwy trajectory on each laser pulse to expose fresh surfaces during the laser-ablation experiments. The pulsed valve was employed to generate beams of 1,2-diaminoethane, 2-methoxyethanol, and 1,2-dimethoxyethane (all used as purchased without further purification) by supersonic expansion of the vapor seeded in helium with a backing pressure of ~40 psi through a 0.5 mm diameter orifice. The second harmonic (532 nm) of a Nd:YAG laser (~40 mJ/pulse) was weakly focused on a ~1 mm diameter spot of the magnesium disk for the generation of metal cations. The laser-produced species containing metal ions and atoms traversed perpendicularly to the supersonic jet stream 20 mm from the ablation sample target, forming a series of metal cations solvated by the title molecules. The nascent complexes and clusters then traveled 14 cm down to the extraction region of the reflectron time-of-flight spectrometer (RTOFMS).

The cation−molecule complexes were accelerated vertically by a high voltage pulse in a two-stage extractor. After extraction, the cluster cations were steered by a pair of horizontal plates and a pair of vertical deflection plates. All of the cluster cations were reflected by the reflectron and finally detected by a dual-plate microchannel plate detector (MCP). For photodissociation experiments, a two-plate mass gate equipped with a high-voltage pulser was used to select desired cluster cations. The mass-selected cluster cations, once arrived at the turn-around region of the reflectron, were irradiated with a collimated beam of a dye laser for photolysis. The parent and nascent daughter cations were reaccelerated by the reflectron electric field and detected by the MCP detector. The dye laser was pumped by a XeCl excimer laser (Lambda-Physik LPX210i/LPD3002). The spectral region of 335−450 nm was covered by the fundamental outputs of the dye laser using *p*-terphenyl, DMQ, BBQ, Stilbene 1, and Coumarin 440. For the spectral region of 230−270 nm, the second harmonic outputs were employed using Coumarin 503 and Coumarin 480. The branching fraction of each fragment was obtained from the corresponding photodissociation difference mass spectrum at different wavelengths.

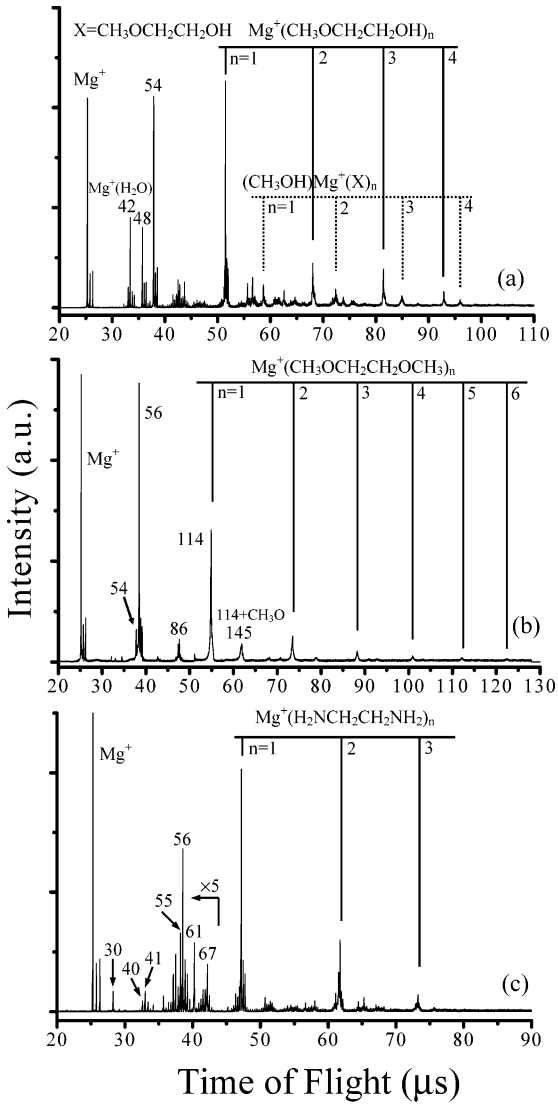

Figure 1. Time-of-flight mass spectra of $Mg^+(2\text{-methoxyethanol})_n$ ($n = 1-4$) (a), $Mg^+(1,2\text{-dimethoxyethane})_n$ ($n = 1-6$) (b), and $Mg^+(1,2\text{-diaminoethane})_n$ ($n = 1-3$) (c). Note that the spectral portion in the flight time range of 20.0−42.5 μs in c is expanded by 5 times for a better view of small peaks.

Results

A. Photoinduced Reaction Patterns. Figure 1 shows the mass spectra of the cationic clusters $Mg^+(HOCH_2CH_2OCH_3)_n$ ($n = 1-4$), $Mg^+(CH_3OCH_2CH_2OCH_3)_n$ ($n = 1-5$), and $Mg^+(H_2NCH_2CH_2NH_2)_n$ ($n = 1-3$). For all of the three systems, the complexes with $n = 1$ are dominant. It is noted that some pronounced thermal reaction products appear in the mass spectra. For $Mg^+(HOCH_2CH_2OCH_3)$ (Figure 1a), numerous products are observed. The two cationic peaks at $m/z = 42$ and 54 are ascribed to $Mg^+(H_2O)$ and $Mg^+(HCHO)$, respectively. Careful examination at the mass spectrum in Figure 1a reveals the presence of $MgOH^+$ (m/z=41). The mass spectrum of $Mg^+(CH_3OCH_2CH_2OCH_3)_n$ in Figure 1b seems cleaner with a smaller number of products. The peak at $m/z = 42$

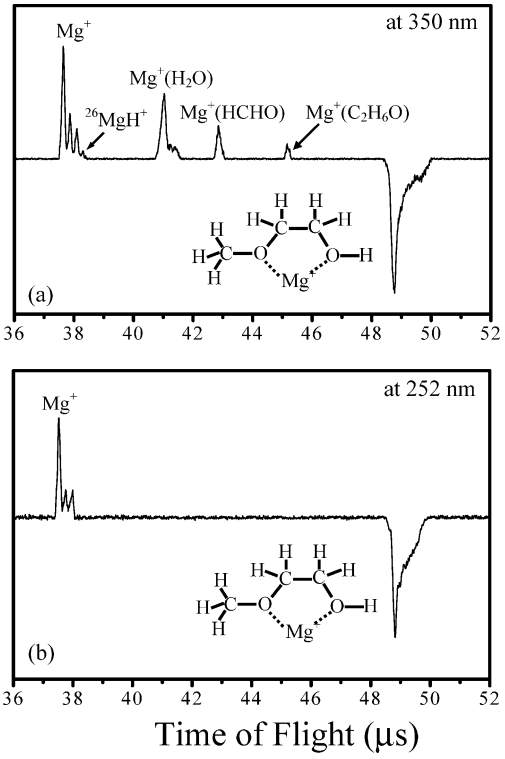

Figure 2. Photodissociation difference mass spectra of Mg^+(2-methoxyethanol) at 350 (a) and 252 nm (b).

$[Mg^+(H_2O)]$ observed in Figure 1a is absent in Figure 1b because of the methyl substitution, whereas the peak at m/z = 54 $[Mg^+(HCHO)]$ (Figure 1a) also appears in Figure 1b although with much lower intensity. Most prominent is the strong peak at m/z = 56 in Figure 1b, which is assigned to $Mg^+(HOCH_3)$ unambiguously. Another peak at m/z = 86 is associated with the loss of C_2H_4 the monosolvated complex $Mg^+(CH_3OCH_2$-$CH_2OCH_3)$. In the mass spectrum of $Mg^+(H_2NCH_2CH_2NH_2)$ (Figure 1c), an even larger number of thermal reaction products are observed. It is noteworthy that these thermal reaction products are also formed for larger clusters in all of the three systems. In addition, the product mass spectra become cleaner as the cluster size increases perhaps because of the increased degrees of freedom for the energy relaxation.

In the present work, the three monosolvated complexes are mass-selected and subjected to photolysis. The mass gate selects a given parent complex in a 5 μs time window. The timings of the mass gate and the photolysis laser are carefully adjusted to ensure that the photofragments are indeed from the parent complex of interest. Sometimes, impurities with a difference of 1 or 2 mass units from the parent complex may also be selected as in the case of $Mg^+(H_2NCH_2CH_2NH_2)$ (Figure 1a). However, even in this case, the mass peak is still dominated by $Mg^+(H_2NCH_2CH_2NH_2)$. As seen below, the photoreaction patterns are in general much simpler than those of the thermal reactions mentioned above owing to the more restricted reactant configurations. The photodissociation difference mass spectra of $Mg^+(HOCH_2CH_2OCH_3)$ at selective wavelengths are presented in Figure 2. Four photofragments are clearly identified at the long wavelength (350 nm), including Mg^+, $Mg^+(H_2O)$, $Mg^+(HCHO)$, and $Mg^+(C_2H_6O)$. Another photofragment MgH^+ is also discernible by the peak at m/z = 27, although it is partially overlapped with the isotopic envelope of Mg^+. As will be discussed below, this species may be from a hydrogen-shift intermediate formed through the abstraction of an H atom by Mg^+ from one of the C−H bonds. Interestingly, all of the

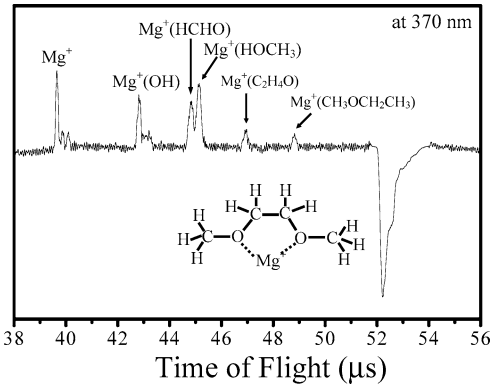

Figure 3. Photodissociation difference mass spectrum of Mg^+(1,2-dimethoxyethane) at 370 nm.

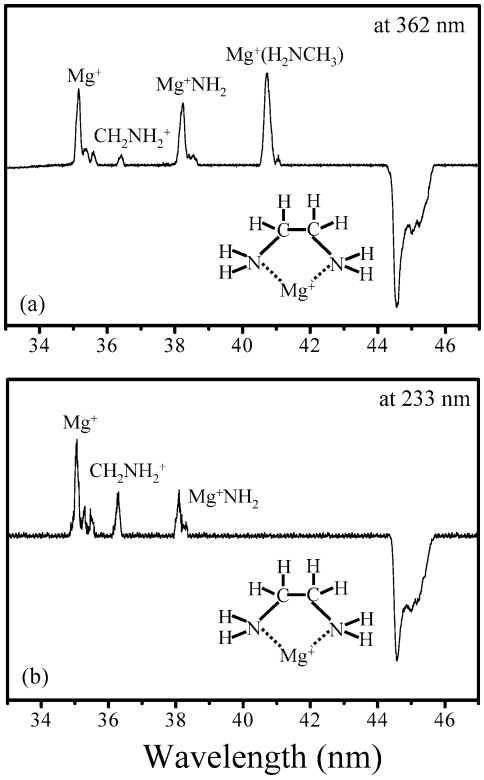

Figure 4. Photodissociation difference mass spectra of Mg^+(1,2-diaminoethane) at 362 (a) and 233 nm (b).

reactive channel photoproducts disappear completely at the short wavelength whereas the nonreactive channel photofragment Mg^+ persists (Figure 2b).

For the sake of comparison, the photolysis of the related complex $Mg^+(CH_3OCH_2CH_2OCH_3)$ has also been studied. Its photodissociation difference mass spectrum at 370 nm is shown in Figure 3. Similarly, aside from the nonreactive channel photofragment Mg^+, five reactive channel photoproducts are observed. Among the reactive channel photoproducts, $Mg^+(HCHO)$ has also been produced from the photolysis of $Mg^+(HOCH_2CH_2$-$OCH_3)$. Other photoproducts are Mg^+OH, $Mg^+(HOCH_3)$, $Mg^+(C_2H_4O)$, and $Mg^+(CH_3OCH_2CH_3)$. Photolysis at short wavelengths has not been carried out, but it is expected to be akin to the case of $Mg^+(HOCH_2CH_2OCH_3)$.

The photoreaction pattern of another bidentate complex $Mg^+(H_2NCH_2CH_2NH_2)$ is displayed in Figure 4. Again, the nonreactive channel photofragment Mg^+ is observed at both long and short wavelengths. For the reactive channel photoproducts, $CH_2NH_2^+$ (m/z = 30) and Mg^+NH_2 (m/z = 40) are

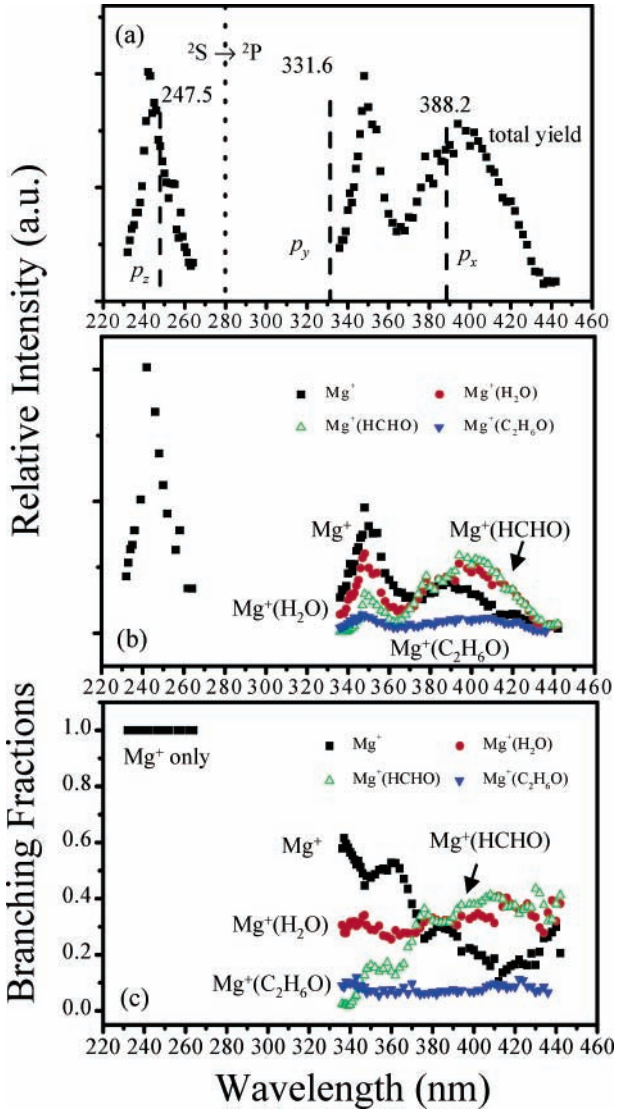

Figure 5. Action spectra (a and b) and branching fraction curves (c) of Mg^+(2-methoxyethanol). The dotted line indicates the atomic transition of Mg^+ ($3^2P \leftarrow 3^2S$) at 280 nm, and the dashed lines denote the absorption spectra calculated using the CIS method.

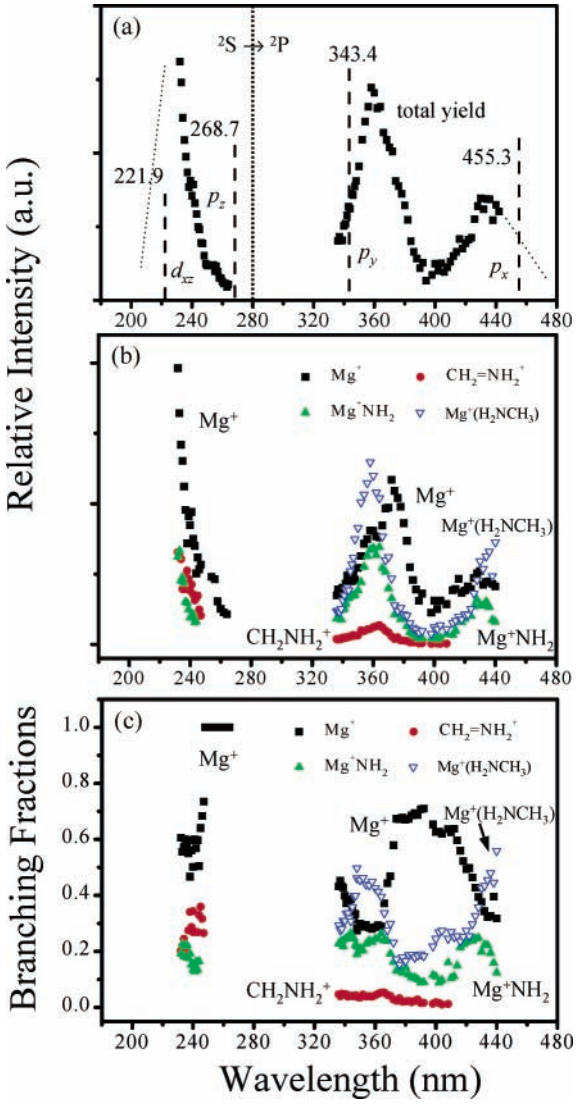

Figure 6. Action spectra (a and b) and branching fraction curves of Mg^+(1,2-diaminoethane). The dashed lines denote the calculated absorption spectra using the CIS method. The thicker dotted line indicates the atomic transition of Mg^+($3^2P \leftarrow 3^2S$) at 280 nm. The thinner dotted lines at the wavelength $<\sim$230 nm and $>\sim$450 nm are for guiding the eye on the two absorption peaks.

formed in the whole wavelength range we have studied, whereas $Mg^+(H_2NCH_3)$ is formed only in the long wavelength region (Figure 4a). It is worth pointing out that the distorted shape of the parent depletion peaks in Figures 2−4 is not due to the depletion of impurities but due to the peak broadening when adopting the mass selection mode in a reflectron time-of-flight mass spectrometer.

B. Photoreaction Action Spectra and Branching Ratio Curves. Figures 5a−c and 6a−c show the photodissociation action spectra and branching ratio curves for $Mg^+(HOCH_2CH_2OCH_3)$ and $Mg^+(H_2NCH_2CH_2NH_2)$, respectively. From Figures 5a and 6a, it is found that the $3^2S \rightarrow 3^2P$ atomic transition of Mg^+ is split to three peaks in the presence of the bidentate ligands. The CIS calculated absorption spectrum of $Mg^+(HOCH_2CH_2OCH_3)$ agrees fairly well with the experimental action spectrum (Figure 5a) in both peak position and peak intensity. One blue-shifted peak centers at ∼245 nm is ascribed to the photoexcitation of the electron at the 3s orbital of Mg^+ to the $3p_z$ orbital, whereas other two red-shifted peaks are associated with $3p_{x,y}$ orbitals of Mg^+. The more red-shifted peak at ∼400 nm corresponds to the excitation of $3P_x$, whereas the other at ∼350 nm is associated with the $3P_y$ excitation.

The action spectrum of $Mg^+(H_2NCH_2CH_2NH_2)$ also exhibits three peaks. However, the calculated spectrum for $Mg^+(H_2NCH_2CH_2NH_2)$ in the same spectral region contains four absorption peaks. Among the four peaks, the most blue-shifted peak at 221.9 nm results from the promotion of the electron from the 3s orbital to the 3d orbital and the other three peaks, from the blue side to the red side, are ascribed to $3P_z$, $3P_y$, and $3P_x$ excitations, respectively. Noticeably, the action spectrum of $Mg^+(H_2NCH_2CH_2NH_2)$ is red-shifted from that of $Mg^+(HOCH_2CH_2OCH_3)$, especially the peak associated with the $3P_x$ excitation. The results described above may be accounted for by the fact that $-NH_2$ is a better electron donor than CH_3O- and $-OH$, which acts to bring up the 3s orbital energy level of Mg^+ and shift the action spectrum to the red.

Photofragment channel-resolved action spectra of $Mg^+(HOCH_2CH_2OCH_3)$ and $Mg^+(H_2NCH_2CH_2NH_2)$ are presented in Figures 5b and 6b, respectively. For $Mg^+(HOCH_2CH_2OCH_3)$, the action spectra of the three reactive channel photoproducts in the long wavelength range are very similar although they differ to some extent from the action spectrum of Mg^+. Similar situation is also held for $Mg^+(H_2NCH_2CH_2NH_2)$; that is, the action spectra

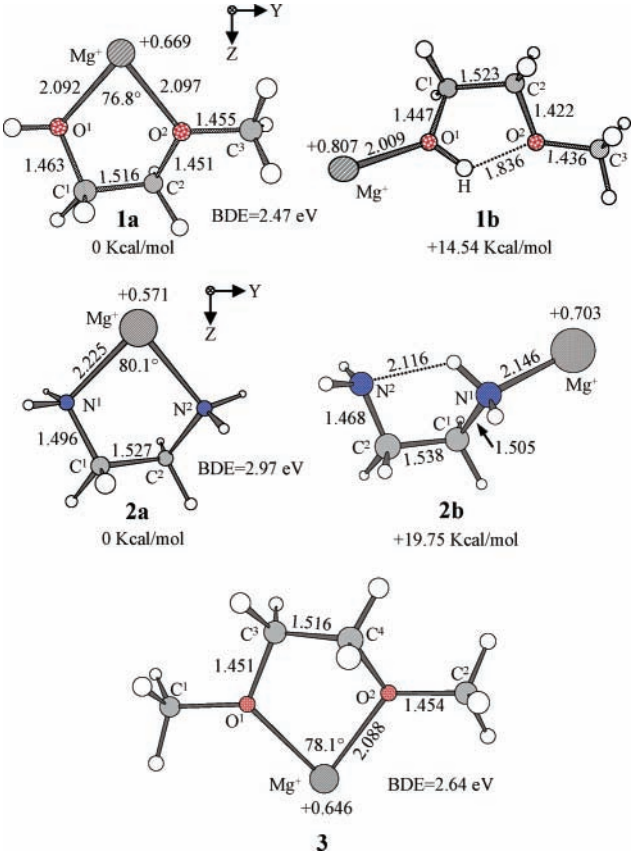

Figure 7. Optimized structures of Mg^+(2-methoxyethanol) (**1a**, **1b**), Mg^+(1,2-diaminoethane) (**2a**, **2b**), and Mg^+(1,2-dimethoxyethane) (**3**). The bond lengths and bond angles are given in angstroms (Å) and degree (°), respectively. "BDE" denotes bond dissociation energy between Mg^+ and the molecule. For each complex, two preferential isomers were optimized. All calculations were performed at the level B3LYP/6-31+G** by using the Gaussian 98 package.

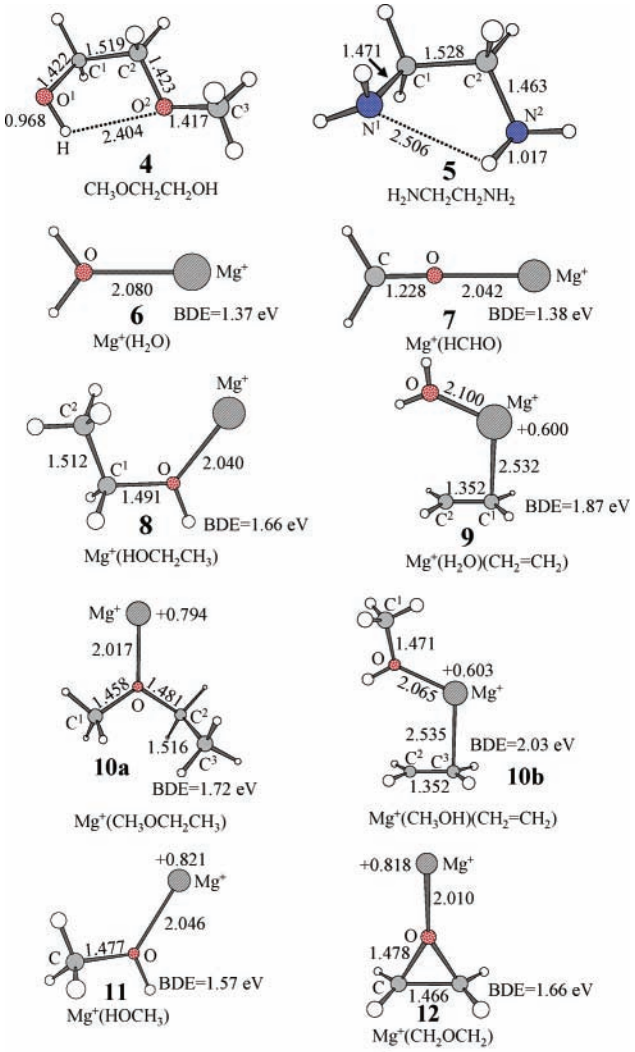

Figure 8. Optimized structures of 2-methoxyethanol (**4**) and 1,2-diaminoethane (**5**) and some possible photoproducts from Mg^+(2-methoxyethanol) (**5**−**8**) and Mg^+(1,2-dimethoxyethane) (**9**−**12**).

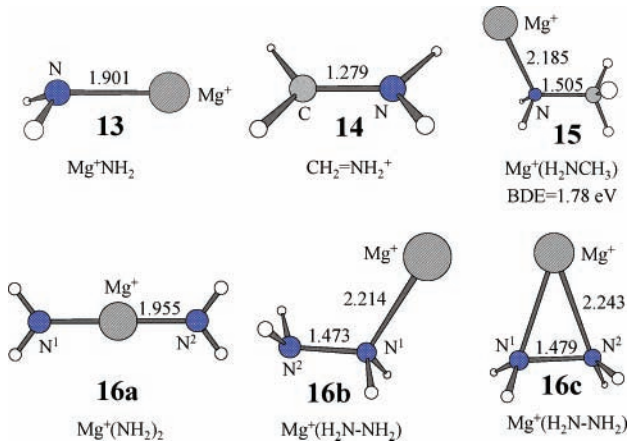

Figure 9. Optimized ground-state structures some possible photoproducts from Mg^+(1,2-diaminoethane) (**13**−**16**).

of the reactive channel products are similar but different from that of Mg^+.

Branching fraction curves of $Mg^+(HOCH_2CH_2OCH_3)$ (Figure 5c) and $Mg^+(H_2NCH_2CH_2NH_2)$ (Figure 6c) have been constructed from the corresponding photofragment channel-resolved action spectra described above. Considering $Mg^+(HOCH_2CH_2OCH_3)$, the branching fraction of Mg^+ increases gradually with the decreasing laser wavelength in the long wavelength range and reaches 100% in the short wavelength range. In the meantime, the branching fractions of the reactive channel photoproducts, especially that of Mg^+(HCHO), show decreasing trends. This suggests that the decomposition tendency of the reactive channel photoproduct cations increases with the increasing photon energy and, thus, contributes to the increasing branching fraction of Mg^+. At a sufficiently short wavelength, all of the reactive channel photoproduct cations are decomposed to Mg^+. Turning to $Mg^+(H_2NCH_2CH_2NH_2)$, the branching pattern is quite different. More or less, the branching fraction curves of the reactive channel photoproducts follow the corresponding action spectra, whereas the branching fraction curve of Mg^+ is somewhat anticorrelated with these action spectra. It appears that the reactive channel photoproducts are mostly from the strong $3^2S \rightarrow 3^2P$ excitation, whereas the nonreactive channel photofragment Mg^+ may be also from the weak excitation of other states.

C. Quantum Mechanics Calculations. Ground-state structures of the three complexes and some of their photofragments are optimized at the B3LYP/6-31+G** level using Gaussian 98 package.[47] Selected results are presented in Figures 7−9. The geometrical parameters, such as bond length, bond angle, atomic charge of Mg^+, bond dissociation energy (BDE), and relative energy are given. The energetics for the relevant photoreactions is obtained on the basis of the calculated energies of the optimized species, which underlies Schemes 1, 3, and 5. In all of the calculations presented here, zero-point energy (ZPE) correction has been taken into account.

SCHEME 1

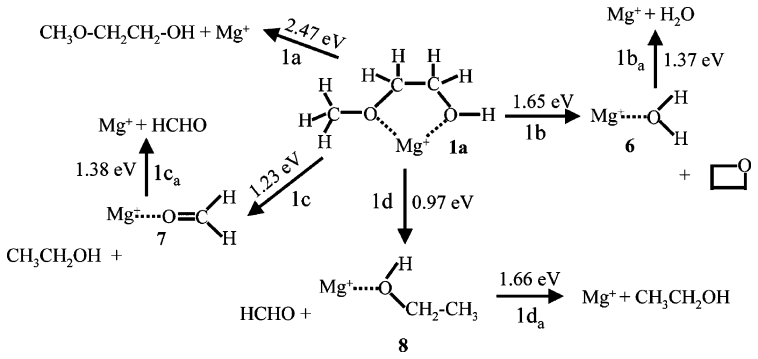

SCHEME 2

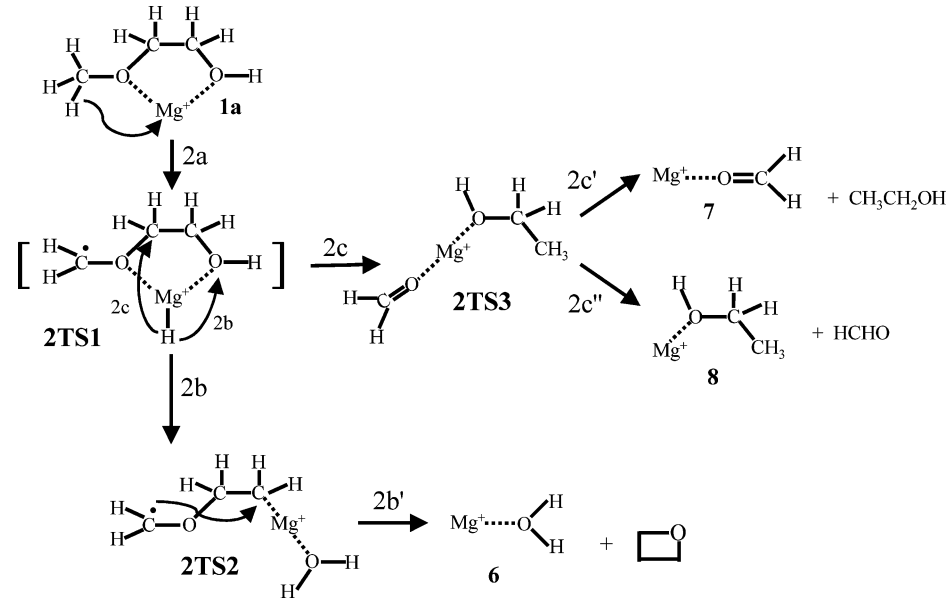

SCHEME 3

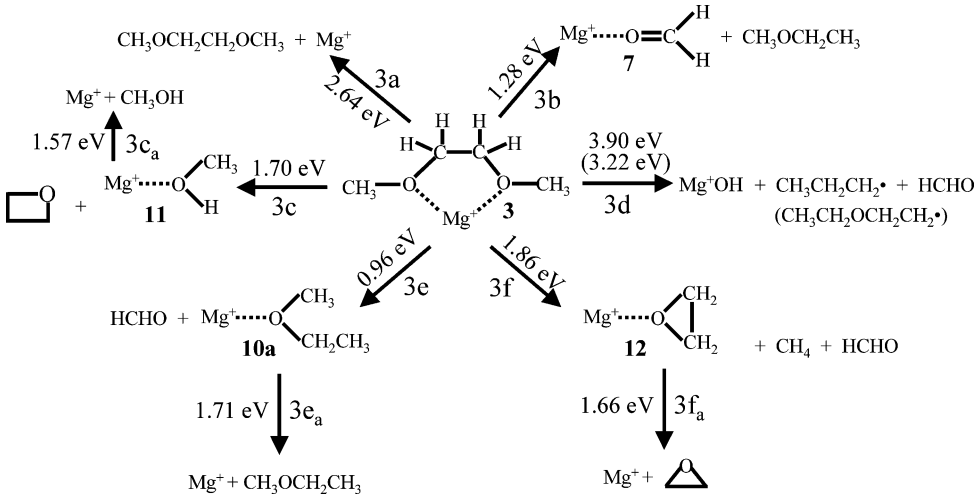

As shown in Figure 7, the most stable ground-state structures of the three complexes (**1a**, **2a**, and **3**) are featured by the chelation of Mg^+ to the two oxygen or nitrogen atoms, forming a five-membered ring. For $Mg^+(HOCH_2CH_2OCH_3)$ and $Mg^+(H_2NCH_2CH_2NH_2)$, two higher-energy monodentate structures (**1b** and **2b**) are also located. Although **1b** and **2b** possess one intrahydrogen bond, they are less stable than **1a** and **2a** by 14.54 and 19.75 kcal/mol, respectively. The atomic charges of Mg^+ in **1a** and **2a** (+0.669 and +0.571) are indeed less positive than those in **1b** and **2b** (+0.807 and +0.703), respectively, owing to the electron donation from the two oxygen atoms in **1a** and the two nitrogen atoms in **2a**. The bond dissociation energies (BDEs) of **1a**, **2a**, and **3** (Figure 7) are calculated to be 2.47, 2.97, and 2.64 eV, respectively. The BDE of **3** (2.64 eV) is 0.17 eV larger than that of **1a** (2.47 eV). This results from the methyl substitution effect, which is also evidenced by the slight shortening of the Mg^+-O bond in **3** (both 2.088 Å) compared to those in **1a** (2.092 and 2.097 Å). Moreover, because

SCHEME 4

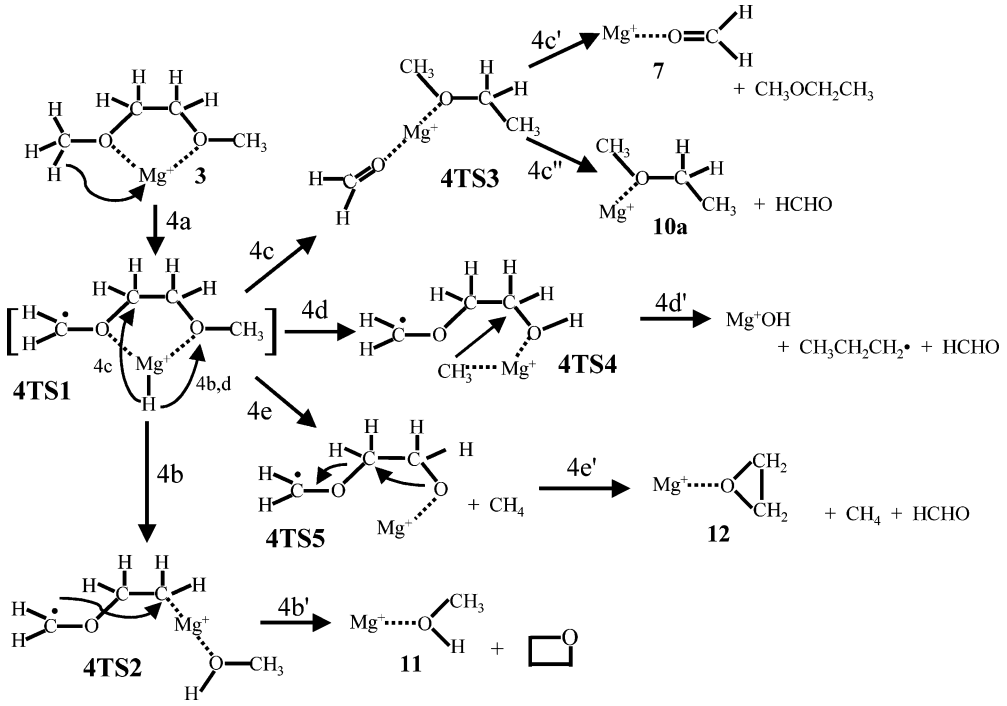

SCHEME 5

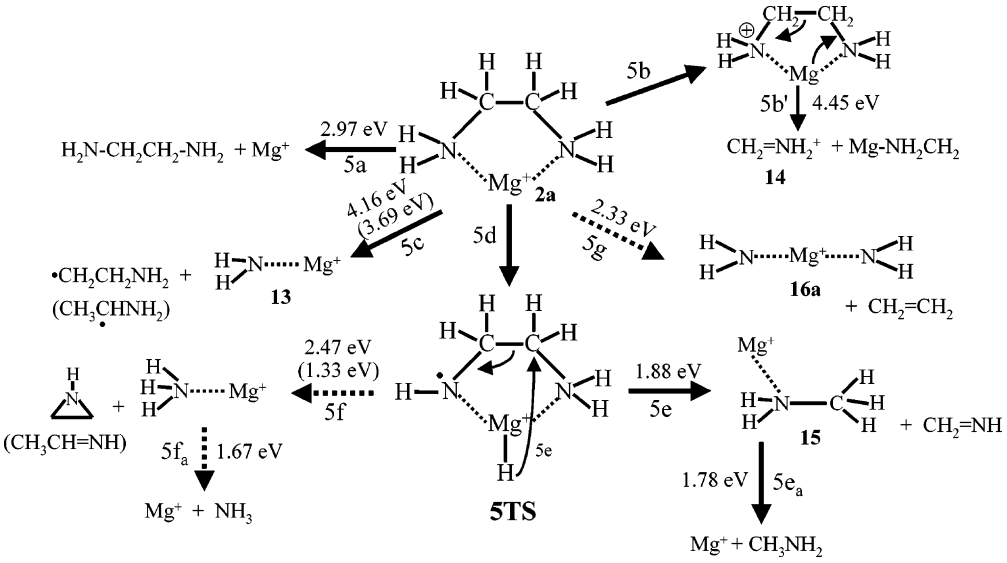

of the methyl substitution, the atomic charge of Mg^+ in **3** (+0.646) is less positive than that in **1a** (+0.669). Of all of the three complexes, **2a** has the highest BDE (2.97 eV). This is evidently due to the stronger donating ability of N as witnessed by the smaller atomic charge of Mg^+ in **2a** (+0.571) than in the other two complexes studied in this work. Such a stronger binding of Mg^+ with the bidentate diaminoethane molecule explains the larger red-shift of the absorption spectrum described above.

The calculation has been extended to the candidate structures of some photoproducts (**6**−**15**) for each complex. The structures of $Mg^+(H_2O)$ (**6**),[3,48] $Mg^+(HCHO)$ (**7**),[2h,49] Mg^+NH_2, $CH_2NH_2^+$, $Mg^+(H_2NCH_3)$ (**13**−**15**),[34a−b] and $Mg^+(HOCH_3)$ (**11**)[50,51] have been calculated previously at different levels, and are consistent with our calculations. The BDEs of **6**−**12** and **15** are between ∼1.3−2.0 eV. The photoproduct with $m/z = 70$ from $Mg^+(HOCH_2CH_2OCH_3)$ (Figure 2a) could be associated with the structure **8** [$Mg^+(HOCH_2CH_3)$] or **9** [$Mg^+(H_2O)(C_2H_4)$]. Similarly, the photoproduct with $m/z = 84$ from $Mg^+(CH_3OCH_2CH_2OCH_3)$ (Figure 3) could be assigned to **10a** [$Mg^+(CH_3OCH_2CH_3)$] or **10b** [$Mg^+(HOCH_3)(C_2H_4)$]. Although the BDEs of **9** and **10b** (1.87 and 2.03 eV) are 0.21 and 0.31 eV larger than those of **8** and **10a** (1.66 and 1.72 eV), respectively, the energies needed for the formation of **9** and **10b** (1.21 and 1.28 eV) are higher than those for **8** and **10a** (0.97 and 0.96 eV). As will be discussed below, the photoproducts with $m/z = 70$ and 84 observed in Figures 2a and 3 are more likely to possess the structures **8** and **10a**, respectively. The species $[Mg^+(NH_2)_2]$ (**16a**) and $Mg^+(H_2N-NH_2)$ (**16b,c**)] are also calculated for comparison.

Discussion

In general, the photofragments of $Mg^+(HOCH_2CH_2OCH_3)$, $Mg^+(CH_3OCH_2CH_2OCH_3)$, and $Mg^+(H_2NCH_2CH_2NH_2)$ can be classified into three types. The evaporation product Mg^+ belongs to the first type, which is present in all of the three complexes

and in the whole wavelength range we have studied. The second type features noncovalent interactions between Mg^+ and close-shell molecules; typical examples are $Mg^+(HCHO)$ and $Mg^+(HOCH_2CH_3)$. For the third type photoproducts, either no Mg^+ is present or covalent interactions between Mg^+ and O/N atoms are involved. This includes Mg^+NH_2 and $CH_2NH_2^+$ from $Mg^+(H_2NCH_2CH_2NH_2)$, MgH^+ from $Mg^+(HOCH_2CH_2OCH_3)$, and Mg^+OH from $Mg^+(CH_3OCH_2CH_2OCH_3)$. Mechanistically, we believe that the second type of photoproducts is rooted in a hydrogen transfer step (or C−H, O−H, and N−H insertions). C−N/C−O insertion photoproducts and hydrogen transfer (or C−H, O−H, and N−H insertions) intermediates constitute the third type. The proposed photoprocesses are all summarized in Schemes 1−5 according to the energetics calculations with zero-point energy correction.

As can be seen from Schemes 1−3, the reaction energies for the formation of the second-type of photoproducts are much lower than the evaporation energies, i.e., BDEs. To be more specific, the BDEs of **1a**, **3**, and **2a** are 2.47, 2.64, and 2.97 eV, respectively, whereas the reaction energies for the formation of the second type of photoproducts are all below 2.0 eV (routes 1b−d, 3b−c, 3e−f, and 5e). In comparison, the reaction energies for the third-type of photoproducts are normally much higher. For example, the reaction energies for the formation of Mg^+OH, Mg^+NH_2, and $CH_2NH_2^+$ are 3.90 (route 3d), 4.16 (route 5c), and 4.45 eV (route 5b), respectively. Clearly, the second type of photoproducts is prone to further dissociation especially in the short wavelength region, resulting in the formation of Mg^+. However, this does not apply to the third type of photoproducts, which in general possess much highr BDEs. In the following, we discuss the three types of the photofragments separately.

A. Evaporation Processes. As mentioned above, the energy required for the evaporative dissociation of the three complexes are calculated to be 2.47, 2.64, and 2.97 eV, respectively. This, together with previous studies,[1−4,33,34] suggests that the evaporation in complexes **1a**, **2a**, and **3** occurs on the ground-state surface because the energies required for the excited-state evaporation processes are far beyond the photon energies we used. Take **1a** for example, the lowest excited state of Mg^+ ^2P is 3.10 eV (∼400 nm) above the ^2S ground state. Thus, the $Mg^+(^2P) + HOCH_2CH_2OCH_3$ asymptote is predicted to lie 5.57 eV above the $Mg^+(HOCH_2CH_2OCH_3)$ ground state. This indicates that any evaporation process induced by a photon with energy lower than 5.57 eV (∼223 nm) should occur on the ground-state surface. Therefore, the initial excitation of $Mg^+(HOCH_2CH_2OCH_3)$ was followed by internal conversion to the ground-state surface, leading to the ultimate evaporation. Also, it should be mentioned that, although Mg^+ observed in the long wavelength range comes mainly from the evaporation of the corresponding complex, further dissociation of Mg^+-bearing photofragments also contributes to the yield of Mg^+ in the short wavelength range.

B. Photoinduced Hydrogen Shift Reactions. As mentioned above, most of the photoproducts from $Mg^+(HOCH_2CH_2OCH_3)$ (**1a**), $Mg^+(CH_3OCH_2CH_2OCH_3)$ (**3**), and $Mg^+(H_2NCH_2CH_2NH_2)$ (**2a**) seem to be derived from common doorway intermediates, the hydrogen shift intermediates. Literally, all of the second type and some of the third type of photoproducts cannot be obtained without hydrogen transfer. The proposed hydrogen-shift mechanism for the three complexes is explicitly inlaid in Schemes 2, 4, and 5. After photoexcitation of Mg^+ to $(Mg^+)^*$, one hydrogen atom is transferred to Mg^+ through C−H or N−H activations. This hydrogen atom can then be used for subsequent reactions. One piece of evidence for the H-shift intermediates is the photoformation of MgH^+ from **1a**. Although this photoproduct has not been observed from the other two complexes, it may be just too weak to be detected.

For the H-shift intermediate **2TS1** from the complex **1a**, as shown in Scheme 2, the H atom on Mg^+ is abstracted from the $-CH_3$ group leaving behind the CH_2O- moiety (route 2a). Remarkably, such an intermediate can account for most of the photoproducts we observed. Depending on which atom (C or O) the H atom attacks, different photoproducts may be formed. For instance, if the H atom is transferred to the O atom of the $-OH$ group, the route 2b will lead to the formation of Mg^+H_2O (**6**). On the other hand, the H attack on the C atom of the ethylene unit results in the breakage of the C−O bond through the route 2c to form **2TS3**. Subsequently, the pathways 2c′ and 2c″ yield Mg^+H_2CO (**7**) and $Mg^+HOCH_2CH_3$ (**8**), respectively.

The hydrogen-shift intermediate from the complex **3** is **4TS1**. Here even more reaction pathways (4b−4e) are accessible as can seen in Scheme 4. Similar to the photoreactions of the complex **1a** described above, however, the C−C bond is still intact. First, through the attack of the $-CH_3$ group by the H atom, **4TS5** is formed with the ejection of CH_4, ultimately giving birth to $Mg^+OCH_2CH_2$ (Mg^+(epoxyethane), **12**). Other structures such as $Mg^+(OCHCH_3)$ can also be envisioned if H shift is possible, which however often involves a high barrier. Second, the attack of the H atom on the C atom of the ethylene moiety opens the pathway 4c. Third, the H atom can also attack the O atom of the $-OCH_3$ group. This brings about two scenarios. The first is the insertion of Mg^+ into the $-CH_2-O$ bond (route 4b), and the other is the CH_3-O bond (route 4d). Different photoproducts Mg^+HOCH_3 (**11**) and Mg^+OH will be formed. It's intriguing that without the methyl substitution cation **12** was absent in the photolysis of **1a**. This might be appreciated from the energy point of view. Without the methyl substitution, the formation energy of **12** from **1a** was calculated to be 2.77 eV (not shown in Scheme 1), which is much higher than those of second-type photoproducts of **1a** (pathways 1b−1d). However, with the methyl substitution, the energy required for forming **12** from **3** (route 3f) is decreased to 1.86 eV, which is comparable with the formation energy of $Mg^+(HOCH_3)$ (1.70 eV for the route 3c). Therefore, the formation process of **12** is less favorable than other reactive processes in **1a**, whereas it becomes competitive with other reactive processes in **3** with the methyl substitution. Another note is the observation of Mg^+OH from **3**, which was not produced from photoreaction of **1a** despite having an end OH group. This arises from the possible insertion of Mg^+ to two available C−O bonds with the CH_3 substitution. It appears that the activation of the C−O bond by Mg^+ is more favorable than that of the O−H bond.[3] Therefore, the photoformation of Mg^+OH is not possible from **1a**.

To some extent, the photochemistry of $Mg^+(H_2NCH_2CH_2NH_2)$ (**2a**) is different. Most noticeably, the C−C bond rupture is more facile owing to the energy compensation of forming strong C═N bonds. In addition, the photoproduct channels seem to be more limited. In fact, $Mg^+(H_2NCH_3)$ (**15**) is the only second type of photoproduct observed from $Mg^+(H_2NCH_2CH_2NH_2)$ (**2a**). Nevertheless, the H-shift mechanism still operates as shown in Scheme 5. What is changed here is that the shifted H atom was directly bonded to N instead of α-C as in the complexes of the glycol derivatives. In such a H-shift intermediate, the H attack on the C elicits the C−C bond cracking followed by the formation of a strong C═N bond. In principle, the H atom could also attack the N atom of NH_2. This would lead to the formation of $Mg^+(NH_3)$ and ring-closed aziridine

CH_2CH_2NH (route 5f), which needs a higher energy (2.47 eV). Although $NH-CH_2-CH_2$ may isomerize to a more stable form $CH_3-CH=NH$, there is likely a high-energy barrier related to the further H-shift in the course en route to $CH_3-CH=NH$.

It is fitting at this point to address why all of the reactive channel photoproducts from $Mg^+(HOCH_2CH_2OCH_3)$ and some from $Mg^+(H_2NCH_2CH_2NH_2)$ observed in the long wavelength region disappear in the short wavelength region. The first explanation coming to mind may be that the photoreactions are state-specific. However, more likely is that the reactive channel photoproduct cations decompose further to Mg^+. In fact, the decomposition has already started even in the long wavelength region. This is evidenced by the fact that the decreasing branching fractions of the photoproducts are accompanied by the increasing branching fraction of Mg^+ (Figure 5c). In addition, the photon energy is much more than enough to induce the reactions and to further decompose the products to Mg^+. According to our calculations, the BDEs and the reaction energies for the formation of **6**−**12** and **15** are found to be in the ranges of 1.3−2.0 and 0.9−1.9 eV, respectively. The sum of the two values for a given photoproduct varies between 2.5 and 3.7 eV, which is within the accessibility of one photon even at the long wavelengths.

We wish to caution that the proposed H-shift mechanisms in Schemes 1−5 need further verifications by separate experiments such as isotopic substitutions. It is nevertheless a plausible hypothesis that explains coherently the experimental results we have obtained so far for the three bidentate complexes.

C. Other Photoreactions. Photolysis of **1a** and **3** has produced predominantly the first and the second type of fragments, which have been discussed above at some length. It turns out that, for $Mg^+(H_2NCH_2CH_2NH_2)$ (**2a**), the third type of photoproducts is also obtained in abundance besides the first and the second type of photofragments. These include $CH_2NH_2^+$ (**13**) and Mg^+NH_2 (**14**). The reaction pathways leading to these photoproducts are depicted in Scheme 5.

The energy required for the cleavage of the C−C bond with the formation of $CH_2NH_2^+$ ($m/z = 30$) and $MgNH_2CH_2$ (route 5b in Scheme 5) is calculated to be 4.45 eV (∼279 nm). Although $CH_2NH_2^+$ is observed at 362 nm (Figure 4a), it's believed to be from the two-photon contribution. The one-photon regime can be accessed only in the short wavelength region. Consistent with these, the intensity of $CH_2NH_2^+$ is rather small and fades away in the long wavelength region, whereas its intensity and branching fraction are much larger in the short wavelength region (Figures 4b and 6c). Bouchoux et al. noticed that $H_2NCH_2CH_2NH_2^{\bullet+}$ loses ammonia at low internal energy, whereas it undergoes the C−C bond cleavage rapidly at higher internal energy.[44] This can be used to explain the photoformation of $CH_2NH_2^+$ in our experiment. The high energy radical cation is produced by photoinduced charge transfer as found in other Mg^+(amine) complexes (route 5b in Scheme 5).[34a−c] The subsequent rearrangement results in the photoproducts (route 5b′) we observed.

Proceeding to the pathway 5c, the formation energy of Mg^+NH_2 and $^\bullet CH_2CH_2NH_2$ is calculated to be 4.16 eV. Apparently, this pathway begins with the insertion of Mg^+ into the C−N bond, followed by the formation of Mg^+NH_2. This product has been observed previously in the photoreactions of Mg^+(methyl- and propylamines) through C−N bond activation.[34b,c] Moreover, similar to the case of $CH_2NH_2^+$, the photoformation of Mg^+NH_2 is not state-specific from $Mg^+(H_2NCH_2CH_2NH_2)$ as well as from Mg^+(methyl- and propylamines). This may be caused by the fact that the three 3p orbitals of Mg^+ are neither parallel nor perpendicular to the C−N bond in three systems. It is worthy of note that $Mg^+(NH_2)_2$ (**16a**) and $Mg^+(H_2N-NH_2)$ (**16b**,**c**) are not observed even though the energetics favors their formation (e.g., the reaction energy for the formation of **16a** is only 2.33 eV (route 5g)). This is understandable because once Mg^+ is inserted into one of the C−N bonds, it will be impossible to have a second insertion. On the other hand, the transfer of the second NH_2 group seems to be rather difficult.

Conclusions

By combining photodissociation spectroscopy and ab initio calculations, We have studied photoinduced reactions of mass-selected bidentate complexes $Mg^+(HOCH_2CH_2OCH_3)$, $Mg^+(CH_3OCH_2CH_2OCH_3)$, and $Mg^+(H_2NCH_2CH_2NH_2)$ in a broad spectral range from 230 to 440 nm. Ab initio calculations are performed on structures of relevant complexes and photofragments, absorption spectra, and energetics of the photoprocesses involved in the experiments. Several points can be made as follows through the present studies.

(1) Three types of photofragments have been observed from $Mg^+(HOCH_2CH_2OCH_3)$, $Mg^+(CH_3OCH_2CH_2OCH_3)$, and $Mg^+(H_2NCH_2CH_2NH_2)$. The first type is the evaporation product Mg^+, which is always produced. Mg^+−molecule complexes represent the second type of photoproducts. This includes all of the reactive channel photoproducts from $Mg^+(HOCH_2CH_2OCH_3)$ and $Mg^+(CH_3OCH_2CH_2OCH_3)$ and $Mg^+(H_2NCH_3)$ from $Mg^+(H_2NCH_2CH_2NH_2)$. Other reactive channel photoproducts, such as Mg^+OH from $Mg^+(CH_3OCH_2CH_2OCH_3)$ and $CH_2NH_2^+$ and Mg^+NH_2 from $Mg^+(H_2NCH_2CH_2NH_2)$ are classified as the third type of photoproducts.

(2) The action spectrum of $Mg^+(H_2NCH_2CH_2NH_2)$ differs from that of $Mg^+(HOCH_2CH_2OCH_3)$ mainly in peak shift; the blue peak is more blue-shifted, and the red peaks are more red-shifted. This reflects the stronger coordination of $N-Mg^+$ than that of $O-Mg^+$ as born out in our quantum mechanics calculations.

(3) The proposed hydrogen-shift mechanism accounts for all of the reactive channel photoproducts from $Mg^+(HOCH_2CH_2OCH_3)$ and $Mg^+(CH_3OCH_2CH_2OCH_3)$, as well as the second type of photoproduct from $Mg^+(H_2NCH_2CH_2NH_2)$. The shift of a hydrogen atom from α-C or N to Mg^+ is at the heart of this mechanism. Being activated, the H atom can search for points of attack and gate reaction channels. As such, the formation of the H-shift intermediates opens paths to a rich variety of photoproducts. The loss of all of the second-type photoproducts in the short wavelength range is attributed to the further decomposition owing to their BDEs being much smaller than the available internal energies after the primary photoreactions. Further experiments such as isotopic substitutions are needed and have been planned to confirm this mechanism.

(4) In contrast to the photoreactions of Mg^+(glycol derivatives), the C−C bond in $Mg^+(H_2NCH_2CH_2NH_2)$ can be shattered following photoactivation. This comes about through a transfer of either an H atom or an electron to Mg^+ directly from the N atom, which is not likely in the photoreactions of Mg^+(glycol derivatives). What is more, as opposed to the absence of direct C−O insertion in the photoreactions of Mg^+(glycol derivatives), straight C−N bond activation is possible in the photoreactions of $Mg^+(H_2NCH_2CH_2NH_2)$, giving rise to $CH_2NH_2^+$ and Mg^+NH_2. As part of the reasons, the direct C−O insertion in Mg^+(glycol derivatives) is perhaps overwhelmed by the facile H-shift photoreactions.

(5) The DFT/B3LYP method has been successfully employed to obtain optimized ground-state geometries of the title com-

plexes and relevant photoproducts. The calculations approximately reproduce the action spectra of the complexes and give reasons for many of our experimental results presented here. In particular, the calculations are valuable for shaping and sorting out the fairly sophisticated reaction mechanisms in these relatively large systems.

Acknowledgment. This work was supported by an RGC grant administered by the UGC of Hong Kong.

References and Notes

(1) (a) Duncan, M. A. *Annu. Rev. Phys. Chem.* **1997**, *48*, 69. (b) Reddic, J. E.; Duncan, M. A. *J. Chem. Phys.* **1999**, *110*, 9948. (c) Reddic, J. E.; Pullins, S. H.; Duncan, M. A. *J. Chem. Phys.* **2000**, *112*, 4974. (d) Yeh, C. S.; Willey, K. F.; Robbins, D. L.; Duncan, M. A. *Int. J. Mass Spectrm. Ion Processes* **1994**, *131*, 307. (e) Scurlock, C. T.; Pullins, S. H.; Duncan, M. A. *J. Chem. Phys.* **1996**, *105*, 3579. (f) Robbins, D. L.; Brock, L. R.; Pilgrim, L. S.; Duncan, M. A. *J. Chem. Phys.* **1995**, *102*, 1481. (g) Kirschner, K. N.; Ma, B.; Bowen, J. P.; Duncan, M. A. *Chem. Phys. Lett.* **1998**, *295*, 204. (h) Yeh, C. S.; Willey, K. F.; Robbins, D. L.; Duncan, M. A. *Chem. Phys. Lett.* **1992**, *196*, 233. (i) Willey, K. F.; Yeh, C. S.; Robbins, D. L.; Pilgrim, J. S.; Duncan, M. A. *J. Chem. Phys.* **1992**, *97*, 8886. (j) Scurlock, C. T.; Pullins, S. H.; Duncan, M. A. *J. Chem. Phys.* **1996**, *104*, 4591. (k) France, M. R.; Pullins, S. H.; Duncan, M. A. *Chem. Phys.* **1998**, *239*, 447. (l) Reddic, J. E.; Duncan, M. A. *Chem. Phys. Lett.* **1999**, *312*, 96. (m) France, M. R.; Pullins, S. H.; Duncan, M. A. *J. Chem. Phys.* **1998**, *109*, 8842. (n) France, M. R.; Pullins, S. H.; Duncan, M. A. *J. Chem. Phys.* **1998**, *108*, 7049. (o) Wesolowski, S. S.; Rollin, A. K.; Schaefer, H. F., III.; Duncan, M. A. *J. Chem. Phys.* **2000**, *113*, 701.

(2) (a) Kleiber, P. D.; Chen, J. *Int. Rev. Phys. Chem.* **1998**, *17*, 1. (b) Ding, L. N.; Young, M. A.; Kleiber, P. D.; Stwalley, W. C.; Lyyra, A. M. *J. Phys. Chem.* **1993**, *97*, 2181. (b) Cheng, Y. C.; Chen, J.; Ding, L. N.; Wong, T. H.; Kleiber, P. D.; Liu, D.-K. *J. Chem. Phys.* **1998**, *104*, 6452. (c) Chen, J.; Cheng, Y. C.; Kleiber, P. D. *J. Chem. Phys.* **1997**, *106*, 3884. (d) Chen, J.; Wong, T. H.; Kleiber, P. D. *Chem. Phys. Lett.* **1997**, *270*, 185. (e) Chen, J.; Wong, T. H.; Cheng, Y. C.; Montgomery, K.; Kleiber, P. D. *J. Chem. Phys.* **1998**, *108*, 2285. (f) Holmes, J. H.; Kleiber, P. D.; Olsgaard, D. A.; Yang, K.-H. *J. Chem. Phys.* **2000**, *112*, 6583. (g) Chen, J.; Wong, T. H.; Kleiber, P. D. *J. Chem. Phys.* **1998**, *109*, 8311. (h) Lu, W.-Y.; Wong, T.-H.; Sheng, Y.; Kleiber, P. D. *J. Chem. Phys.* **2002**, *117*, 6970. (i) Lu, W.-Y.; Kleiber, P. D. *J. Chem. Phys.* **2001**, *114*, 10288. (j) Lu, W.-Y.; Kleiber, P. D. *Chem. Phys. Lett.* **2001**, *338*, 291. (k) Lu, W.-Y.; Acar, M.; Kleiber, P. D. *J. Chem. Phys.* **2002**, *116*, 4847.

(3) (a) Misaizu, F.; Sanekata, M.; Tsukamoto, K.; Fuke, K. Iwata, S. *J. Phys. Chem.* **1992**, *96*, 8259. (b) Misaizu, F.; Sanekata, M.; Tsukamoto, K.; Fuke, K. Iwata, S. *J. Chem. Phys.* **1994**, *100*, 1161. (c) Watanabe, H.; Iwata, S.; Hashimoto, K.; Misaizu, F.; Fuke, K. *J. Am. Chem. Soc.* **1995**, *117*, 755. (d) Sanekata, M.; Misaizu, F.; Fuke, F.; Iwata, S.; Hashimoto, K. *J. Am. Chem. Soc.* **1995**, *117*, 747. (e) Yoshida, S.; Daigoku, K.; Okai, N.; Takahata, A.; Sabu, A.; Hashimoto, K.; Fuke, K. *J. Chem. Phys.* **2002**, *117*, 8657. (f) Fuke, K.; Hashimoto, K.; Iwata, S. *Adv. Chem. Phys.* **1999**, *110*, 431.

(4) (a) Shen, M. H.; Farrar, J. M. *J. Chem. Phys.* **1991**, *94*, 3322. (b) Qian, J.; Midey, A. J.; Donnelly, S. G.; Lee, J. I.; Farrar, J. M. *Chem. Phys. Lett.* **1995**, *244*, 414. (c) Sperry, D. C.; Lee, J. I.; Farrar, J. M. *Chem. Phys. Lett.* **1999**, *304*, 350. (d) Sperry, D. C.; Midey, A. J.; Lee, J. I.; Qian, J.; Farrar, J. M. *J. Chem. Phys.* **1999**, *111*, 8469. (e) Lee, J. I.; Sperry, D. C.; Farrar, J. M. *J. Chem. Phys.* **2001**, 114, 6180. (f) Lee, J. I.; Farrar, J. M. *J. Phys. Chem. A* **2002**, *106*, 11882.

(5) (a) Shoeib, T.; Siu, K. W. M.; Hopkinson, A. C. *J. Phys. Chem. A* **2002**, *106*, 6121. (b) Shoeib, T.; Hopkinson, A. C.; Siu, K. W. M. *J. Phys. Chem. B* **2001**, *105*, 12399.

(6) Dickins R. S.; Aime, S.; Batsanov, A. S.; Beeby, A.; Botta, M.; Bruce, J. I.; Howard, J. A. K.; Love, C. S.; Parker, D.; Peacock, R. D.; Puschmann, H. *J. Am. Chem. Soc.* **2002**, *124*, 12697.

(7) Dunbar, R. C. *J. Phys. Chem. A* **2000**, *104*, 8067.

(8) Hoyau, S.; Ohanessian, G. *J. Am. Chem. Soc.* **1997**, *119*, 2016.

(9) Cerda, B. A.; Wesdemiotis, C. *J. Am. Chem. Soc.* **1995**, *117*, 9734.

(10) Lei, Q. P.; Amster, I. J. *J. Am. Soc. Mass Spectrom.* **1996**, *7*, 722.

(11) (a) Wong, C. H. S.; Siu, F. M.; Ma, N. L.; Tsang, C. W. *J. Mol. Struct. (THEOCHEM)* **2002**, *588*, 9.

(12) Moision, R. M.; Armentrout, P. B. *J. Phys. Chem. A* **2002**, *106*, 10350.

(13) (a) Luna, A.; Amekraz, B.; Tortajada, J.; Morizur, J. P.; Alcami, M.; Mo, O.; Yanez, M. *J. Am. Chem. Soc.* **1998**, *120*, 5411. (b) Rodriguez-Santiago, L.; Sodupe, M.; Tortajada, J. *J. Phys. Chem. A* **2001**, *105*, 5340. (c) Boutreau, L.; Toulhoat, P.; Tortajada, J.; Luna, A.; Mo, O.; Yanez, M. *J. Phys. Chem. A* **2002**, *106*, 9359. (d) Boutreau, L.; Leon, E.; Rodriguez-Santiago, L.; Toulhoat, P.; Mo, O.; Tortajada, J. *J. Phys. Chem. A* **2002**, *106*, 10563. (e) Luna, A.; Amekraz, B.; Tortajada, J.; Morizur, J.-P.; Alcami, M.; Mo, O.; Yanez, M. *J. Phys. Chem. A* **2000**, *104*, 3132. (f) Alcami, M.; Luna, A.; Mo, O.; Yanez, M.; Luna, A.; Morizur, J.-P.; Tortajada, J. *J. Phys. Chem. A* **1998**, *102*, 10120. (g) Luna, A.; Morizur, J.-P.; Tortajada, J.; Alcami, M.; Mo, O.; Yanez, M. *J. Phys. Chem. A* **1998**, *102*, 4652. (h) Boutreau, L.; Leon, E.; Luna, A.; Toulhoat, P.; Tortajada, J. *Chem. Phys. Lett.* **2001**, *338*, 74. (i) Rodriguez-Santiago, L.; Tortajada, J. *Int. J. Mass Spectrom.* **2002**, *1*, 12147. (j) Tortajada, J.; Leon, E.; Morizur, J.-P.; Luna, A.; Mo, O.; Yanez, M. *J. Phys. Chem.* **1995**, *99*, 13890.

(14) (a) Hoyau, S.; Ohanessian, G. *Chem. Eur. J.* **1998**, 4, 1561. (b) Hoyau, S.; Ohanessian, G. *Chem. Phys. Lett.* **1997**, *280*, 266.

(15) Marino, T.; Russo, N.; Toscano, M. *Inorg. Chem.* **2001**, *40*, 6439.

(16) Bertran, J.; Rodriguez-Santiago, L.; Sodupe, M. *J. Phys. Chem. B* **1999**, *103*, 2310.

(17) (a) Rodgers, M. T.; Armentrout, P. B. *J. Am. Chem. Soc.* **2000**, *122*, 8548. (b) Ray, D.; Feller, D.; More, M. B.; Glendening, E. D.; Armentrout, P. B. *J. Phys. Chem.* **1996**, *100*, 16116. (c) More, M. B.; Ray, D.; Armentrout, P. B. *J. Phys. Chem.* **1997**, *101*, 831. (d) More, M. B.; Ray, D.; Armentrout, P. B. *J. Phys. Chem.* **1997**, *101*, 7007. (e) More, M. B.; Ray, D.; Armentrout, P. B. *J. Phys. Chem.* **1997**, *101*, 4254. (f) Koizumi, H.; Zhang, X. G.; Armentrout, P. B. *J. Phys. Chem. A* **2001**, *105*, 2444. (g) Rodgers, M. T.; Armentrount, P. B. *J. Phys. Chem. A* **1999**, *103*, 4955.

(18) Ryzhov, V.; Dunbar, R. C. *J. Am. Chem. Soc.* **1999**, *121*, 2259.

(19) Hill, S. E.; Feller, D. Glendening, E. D. *J. Phys. Chem. A* **1998**, *102*, 3813.

(20) Burk, P.; Koppel, I.; Koppel, I.; Kurg. R.; Gal, J.; Maria, P.; Herreros, M.; Notario, R.; Abboud, J. M.; Anvia, F.; Taft, R. W. *J. Phys. Chem. A* **2000**, *104*, 2824.

(21) Abirami, S.; Ma, N. L.; Goh, N. K. *Chem. Phys. Lett.* **2002**, *359*, 500.

(22) Feller, D.; Apra, E.; Nichols, J. A.; Bernholdt, D. E. *J. Chem. Phys.* **1996**, *105*, 1940.

(23) Liau, Y.-H.; Su, T.-M. *J. Am. Chem. Soc.* **1992**, *114*, 9169.

(24) Boehme, C.; Coupez, B.; Wipff, G. *J. Phys. Chem. A* **2002**, *106*, 6487.

(25) Wu, H.-F.; Brodbelt, S. *J. Am. Chem. Soc.* **1994**, *116*, 6418.

(26) Sauer, J. *Chem. Rev.* **1989**, *89*, 199.

(27) Dougherty, D. A. *Science* **1996**, *271*, 163.

(28) Backvall, J.-E.; Bokman, F.; Blomberg, M. R. A. *J. Am. Chem. Soc.* **1992**, *114*, 534.

(29) Cerda, B. A.; Hoyau, S.; Ohanessian, G.; Wesdemiotis, C. *J. Am. Chem. Soc.* **1998**, *120*, 2437.

(30) (a) Hu, P.; Gross, M. L. *J. Am. Chem. Soc.* **1992**, *114*, 9161. (b) Hu, P.; Gross, M. L. *J. Am. Chem. Soc.* **1992**, *114*, 9153. (c) Hu, P.; Gross, M. L. *J. Am. Chem. Soc.* **1993**, *115*, 8821. (d) Hu, P.; Sorensen, C.; Gross, M. L. *J. Am. Soc. Mass Spectrom.* **1995**, *6*, 1079.

(31) Saraswathi, M.; Miller, J. *J. Am. Soc. Mass Spectrom.* **1996**, *7*, 42.

(32) (a) Remko, M.; Rode, B. M. *Chem. Phys. Lett.* **2000**, *316*, 489. (b) Remko, M. *Mol. Phys.* **1997**, *91*, 929.

(33) (a) Liu, H. C.; Wang, C. S.; Guo, W. Y.; Wu, Y. D.; Yang, S. H. *J. Am. Chem. Soc.* **2002**, *124*, 3794. (b) Yang, X.; Hu, Y. H.; Yang, S. H. *J. Phys. Chem. A* **2000**, *104*, 8496. (c) Yang, X.; Liu, H. C.; Yang, S. H. *J. Chem. Phys.* **2000**, *113*, 3111. (d) Yang, X.; Gao, K. L.; Liu, H. C.; Yang, S. H. *J. Chem. Phys.* **2000**, *112*, 10236. (e) Liu, H. C.; Guo, W. Y.; Yang, S. H. *J. Chem. Phys.* **2001**, *115*, 4612.

(34) (a) Guo, W. Y.; Liu, H. C.; Yang, S. H. *J. Chem. Phys.* **2002**, *117*, 6061. (b) Guo, W. Y.; Liu, H. C.; Yang, S. H. *J. Chem. Phys.* **2002**, *116*, 2896. (c) Yang, S. H. et al. in preparation. (d) Guo, W. Y.; Liu, H. C.; Yang, S. H. *J. Chem. Phys.* **2002**, *116*, 9690.

(35) (a) Chu, I.-H.; Dearden, D. V. *J. Am. Chem. Soc.* **1995**, *117*, 8197. (b) Chu, I.-H.; Zhang, H.; Dearden, D. V. *J. Am. Chem. Soc.* **1993**, *115*, 5736. (c) Zhang, H.; Dearden, D. V. *J. Am. Chem. Soc.* **1992**, *114*, 2754. (d) Zhang, H.; Chu, I.-H.; Leming, S.; Dearden, D. V. *J. Am. Chem. Soc.* **1991**, *113*, 7415.

(36) Li, Y.; Baer, T. *J. Phys. Chem. A* **2002**, *106*, 8658.

(37) Ruttink, P. J. A.; Burgers, P. C.; Fell, L. M.; Terlouw, J. K. *J. Phys. Chem. A* **1998**, *102*, 2976.

(38) Audier, H. E.; Milliet, A.; Leblanc, D.; Morton, T. H. *J. Am. Chem. Soc.* **1992**, *114*, 2020.

(39) Cao, J. R.; George, M.; Holmes, J. L.; Sirois, M.; Terlouw, J. K.; Burgers, P. C. *J. Am. Chem. Soc.* **1992**, *114*, 2017.

(40) Burgers, P. C.; Holmes, J. L.; Hop, C. E. C. A.; Postma, R.; Ruttink, P. J. A.; Terlouw, J. K. *J. Am. Chem. Soc.* **1987**, *109*, 7315.

(41) Biermann, H. W.; Morton, T. H. *J. Am. Chem. Soc.* **1983**, *105*, 5025.

(42) Thissen, R.; Alcaraz, C.; Dutuit, O.; Mourgues, P.; Chamot-Rooke, J.; Audier, H. E. *J. Phys. Chem. A* **1999**, *103*, 5049.

(43) Milliet, A.; Sozzi, G.; Audier, H. E. *Org. Mass Spectrom.* **1992**, *27*, 787.

(44) Bouchoux, G.; Choret, N.; Milliet, A.; Rempp, M.; Terlouw, J. K. *Int. J. Mass Spectrom.* **1998**, *179/180*, 337.

(45) Burgers, P. C.; Fell, L. M.; Milliet, A.; Rempp, M.; Ruttink, P. J. A.; Terlouw, J. K. *Int. J. Mass Spectrom.* **1997**, *167/168*, 291.

(46) (a) Yates, B. F.; Bouma, W. J.; MacLeod, J. K.; Radom, L. *J. Chem. Soc., Chem. Commun.* **1987**, 207. (b) Yates, B. F.; Bouma, W. J.; Radom, L. *J. Am. Chem. Soc.* **1984**, *106*, 5805.

(47) Frisch, M. J.; Trucks, G. W.; Schlegel, H. B.; Scuseria, G. E.; Robb, M. A.; Cheeseman, J. R.; Zakrzewski, V. G.; Montgomery, J. A., Jr.; Stratmann, R. E.; Burant, J. C.; Dapprich, S.; Millam, J. M.; Daniels, A. D.; Kudin, K. N.; Strain, M. C.; Farkas, O.; Tomasi, J.; Barone, V.; Cossi, M.; Cammi, R.; Mennucci, B.; Pomelli, C.; Adamo, C.; Clifford, S.; Ochterski, J.; Petersson, G. A.; Ayala, P. Y.; Cui, Q.; Morokuma, K.; Malick, D. K.; Rabuck, A. D.; Raghavachari, K.; Foresman, J. B.; Cioslowski, J.; Ortiz, J. V.; Stefanov, B. B.; Liu, G.; Liashenko, A.; Piskorz, P.; Komaromi, I.; Gomperts, R.; Martin, R. L.; Fox, D. J.; Keith, T.; Al-Laham, M. A.; Peng, C. Y.; Nanayakkara, A.; Gonzalez, C.; Challacombe, M.; Gill, P. M. W.; Johnson, B. G.; Chen, W.; Wong, M. W.; Andres, J. L.; Head-Gordon, M.; Replogle, E. S.; Pople, J. A. *Gaussian 98*, revision A.7M; Gaussian, Inc.: Pittsburgh, PA, 1998.

(48) Bauschlicher, C. W., Jr.; Sodupe, M.; Partridge, H. *J. Chem. Phys.* **1992**, *96*, 4453.

(49) (a) Bauschlicher, C. W., Jr.; Partridge, H. *J. Phys. Chem.* **1991**, *95*, 3946. (b) Partridge, H.; Bauschlicher, C. W., Jr. *J. Phys. Chem.* **1992**, *96*, 8827.

(50) Lu, W.; Yang, S. H. *J. Phys. Chem. A* **1998**, *102*, 825.

(51) Andersen, A.; Muntean, F.; Walter, D.; Rue, C.; Armentrout, P. B. *J. Phys. Chem. A* **2000**, *104*, 692.